

Algorithm Theoretical Basis Document: NISAR L3 Ice Sheet and Glacier Products

Revision 1

May 23, 2022

Ian Joughin, Eric Rignot, Rick Forster, Alex Gardner, and Bernd Scheuchl

© All rights reserved

The NISAR Algorithm Theoretical Basis Documents (ATBDs) provide the physical and mathematical descriptions of algorithms used in the generation of NISAR science data products. The ATBDs include descriptions of variance and uncertainty estimates and considerations of calibration and validation, exception control and diagnostics. Internal and external data flows are also described.

The NISAR ATBDs were reviewed by a NASA Headquarters review panel in TBD with initial public release later in TBD. The current version is Revision A. The ATBDs may undergo additional version updates after NISAR launch.

TABLE OF CONTENTS

1	INTRODUCTION.....	1
1.1	Purpose of Document	1
1.2	Scope of the Document	1
1.3	Applicable and Reference Documents.....	1
1.3.1	Background and Science Objectives	1
1.4	Product/Algorithm Objectives	2
1.4.1	Measurement Approach.....	2
1.4.2	Tidal Displacement.....	4
1.4.3	Glacier Estimates.....	5
1.5	Instrument Characteristics	5
1.6	Heritage and Current Systems.....	6
2	THEORETICAL BASIS OF ALGORITHM.....	7
2.1.1	Speckle Tracking - Caveats for Velocity Estimation.....	7
2.1.2	Interferograms – Caveats for Velocity Estimation.....	8
2.2	Definition of Quantities Used in Velocity and Grounding-Line Estimation	9
2.2.1	Raw Speckle Tracked Offsets.....	9
2.2.2	Raw Interferometric Phase.....	9
2.2.3	Calibrated Offsets and Phase.....	9
2.3	Velocity Estimates at a Point.....	10
2.3.1	Ice Velocity Derived from Speckle Tracking Along a Single Orbit Track	10

2.4	Ice Velocity Derived from Speckle Tracking and Interferometry Along Single Orbit Track.....	12
2.5	Ice Velocity Derived from Interferometry from Crossing Orbits with Surface-Parallel Flow.....	12
2.6	Ice Velocity Derived from Speckle Tracking from Crossing Orbits with Surface-Parallel Flow	14
2.7	Ice Velocity Mosaicking	<u>15</u>
2.7.1	Combined Estimate	15
2.7.2	Feathering	<u>17</u>
2.7.3	Final Product.....	17
2.8	Calibration.....	<u>18</u>
3	References.....	<u>19</u>

Deleted: 14

Deleted: 16

Deleted: 17

Deleted: 18

1 INTRODUCTION

1.1 Purpose of Document

This document is the Algorithm Theoretical Basis Document (ATBD) for the NISAR ice-sheet and glacier L3 products.

1.2 Scope of the Document

This document describes the theoretical basis algorithms used to determine ice-sheet velocity using a combination of speckle-tracking and interferometric phase. By way of explanation, a basic implementation is outlined. The same set of core algorithms could be implemented with variations on the approach described here.

1.3 Applicable and Reference Documents

Applicable documents levy requirements on areas addressed in this document. Reference documents provide additional information to readers. In case of conflict between the applicable documents and this document, the Project shall review the conflict to find the most effective resolution.

Applicable Documents

- AD1: NISAR Calibration and Validation Plan, JPL D-TBD, June 3, 2016.
- AD2: NISAR Science Data Management and Archive Plan, JPL D-80828, June 1, 2016.
- AD3: NISAR Science Management Plan, JPL D-76340, May 29, 2016.
- AD4: NISAR NASA SDS Software Management Plan, JPL D-95656, January 2017.

Reference Documents

- RD1: NISAR NASA SDS Product Description, JPL D-95672, January 2017.
- RD2: NISAR NASA SDS ATBD, JPL D-95677, January 2017.

1.3.1 Background and Science Objectives

A major objective for NISAR is to collect data to measure velocity over the Greenland and Antarctic ice sheets through time. These same data will be used to determine the time-varying position of the grounding line around Antarctica and on floating ice tongues in Greenland. Thus, the project-produced products are designed to demonstrate and validate the following requirements:

L2 Requirement 445: The NISAR project shall measure the vertical differential displacement of all floating ice shelves and ice tongues with vertical accuracy of 100 mm at 100-m resolution annually (> 95% coverage) and monthly (>50% coverage).

L2 Requirement 667: The NISAR Project shall measure ice sheet (> 90% coverage, including both poles) and glaciers and ice-caps (> 80% coverage) horizontal velocity each cold season to an accuracy better than the sum of 3% of the horizontal velocity magnitude and 1 m/yr (1-sigma), at 100-m resolution in areas of slow deformation (< 50 m/yr).

L2 Requirement 668: The NISAR Project shall measure ice sheet horizontal velocity (90% coverage, including both poles) to an accuracy better than 3% of the horizontal velocity magnitude plus 5 m/yr (1-sigma), at 250-m resolution each cold season in areas of fast deformation (>50 m/yr).

L2 Requirement 738: The NISAR Project shall measure time-varying horizontal velocities of ice-sheets at near-weekly sampling intervals in areas of potential rapid (e.g., outlet glaciers) or seasonal change to an accuracy better than 3% of the horizontal velocity magnitude plus 10 m/yr (1-sigma) at 500-m resolution (> 80% coverage).

1.4 Product/Algorithm Objectives

The Science Team (ST) and the Project Science Team (PST) shall produce the following ice-sheet demonstration/validation products

- Ice sheet velocity products at time scales of 12-days to a year for validation purposes. Examples of such products are velocity maps covering the GPS validation sites, areas with that overlap with coverage provided by other sensors, and stationary areas adjacent to the ice sheet (e.g., bedrock outcrops).
- Differential tidal displacement maps to validate grounding line requirements.
- Velocity estimates to validate the mountain glacier measurement goals.
- A limited set of demonstration products within budgetary limitations.

These products are designed to validate the Level-2 and by extension the Level-1 requirements, but not to completely fulfill them [AD-1]. While data will be collected to meet the requirement throughout the mission, the bulk of the processing to fully meet the requirements will be carried out by the scientific community at large, with funding external to the project [AD1-4].

1.4.1 Measurement Approach

For slow-moving areas (<50 m/yr) and some fast moving areas where the data are conducive to such measurement, horizontal velocity will be measured using radar-line-of sight determined from the interferometric phase from at least two crossing orbit tracks (i.e., ascending/descending) under the assumption that flow is parallel to the known surface [Joughin *et al.*, 1998]. An advantage of this technique is that the data are relatively high-resolution (<100 m) and the phase noise is low (<~2 cm). A major disadvantage is that for fast moving areas it is difficult or impossible to unwrap the phase. Another issue is regions where there is significant ionospheric activity such that the spatially variable path delay introduces large interferometric

phase errors (several m/yr errors). For NISAR, these errors will largely be removed using split-spectrum processing applied to the 80-MHz-bandwidth data (see Level-2 product algorithms).

In areas where the motion is too fast for interferometric phase measurements, velocity will be determined using the azimuth and range offsets derived by cross-correlating patches from pairs of image to determine displacements between image acquisitions [Gray *et al.*, 1998; Michel and Rignot, 1999]. Although image features can improve correlation, this technique works best when the speckle patterns are well correlated; hence this technique is often called speckle tracking. Advantages to this method are that velocity estimates can be derived from a pair of images collected along a single orbit track (i.e., ascending or descending only orbits) and it can be used to measure extreme motion (>10 km/yr). Because the technique uses image chips several 10s of pixels in dimension, the spatial resolution is much poorer (~ 200 m) than phase estimates. Since displacement is resolved to within a fraction (i.e., $\sim 1/20$ of a several-meter pixel) of a range or azimuth pixel, accuracy also is much less than phase estimates, which resolve motion to a fraction of NISAR's 24-cm wavelength).

In polar regions, ionospheric distortion can be severe, particularly for the azimuth offsets. This distortion can produce errors of more than 100 m/yr in some locations in speckle-tracked estimates. This problem can be mitigated by neglecting the heavily contaminated azimuth offsets and using only the range offsets from crossing orbits as described below. This type of estimate is analogous to an interferometric phase estimate from crossing orbits, except the line of sight displacements are derived from range offsets.

The requirements for fast and slow motion reflect the fact that lower-resolution speckle tracking is best suited to measuring fast-flowing outlet glaciers, while interferometric phase is ideal for the slow-flowing interior. Although the 50 m/yr distinction between slow and fast flow in the requirements is aimed at separating the areas where each technique should work the best, in many cases interferometric phase will still work in considerably faster-flowing areas (up to about 500 m/yr for NISAR). Thus, no single velocity threshold can cleanly separate the regions where phase fails and speckle-tracking must be used. For example, with RADARSAT phase can sometimes be unwrapped on smooth ice shelves at speeds approaching 1000 m/yr. By contrast, for some regions on the ice sheets where the speeds are less than 100 m/yr, there are strong phase gradients where ice flows over bumps that make phase unwrapping difficult or impossible. As a result, for all of the velocity related requirements, at each point on the ice sheet, the corresponding requirement will be met using the best available combination of interferometric phase and speckle-tracked offsets. The different temporal and spatial resolutions specified in the requirements reflects the amount of spatial and temporal averaging necessary to meet each requirement.

The basic algorithmic approach follows earlier approaches [Joughin, 2002; Mouginot *et al.*, 2017]. Specifically, at each point in the output grid, the algorithm will cycle through the various options:

- 1) Range-azimuth offsets from a single orbit track,
- 2) Unwrapped phase (for range) with azimuth offsets from a single orbit track,
- 3) Range-range offsets from crossing orbit tracks, and
- 4) Unwrapped phase-phase data from crossing orbits.

At each point in the output, all of the viable combinations will be calculated. Estimated errors for each type of velocity estimate will be used to weight the results to produce an optimal inverse-error weighted average for the horizontal components of velocity. All of these combinations have been widely used [Joughin *et al.*, 2010; Rignot *et al.*, 2011b; Mouginot *et al.*, 2017], with recent work demonstrating the range-range offsets combination [Joughin *et al.*, 2018]. This latter combination is particularly attractive for NISAR because a) the 80-MHz mode provides considerably finer range (~ 2.5 m) than azimuth (~ 7 m) resolution, b) there will be ample ascending/descending coverage, and c) relative to azimuth offsets, the range offsets are less affected by ionospheric distortion. Hence, the range-range offsets combination likely will be the dominant contributor to velocity estimates in region of fast flow. All of the above methods will be implemented, but any of them can be selectively turned off (e.g., methods 1&2 where azimuth offsets add no improvement to the derived estimates.) For much of the processing there will be no need to explicitly turn estimates off as poorer quality data will be de-emphasized through the inverse-error weighting.

All ice-sheet velocity maps will be produced on polar stereographic grids at a posting of 100 m (actual resolution in faster-moving regions will be 250 m or better.) Consistent with the existing products, the Greenland map-projection will use a standard latitude of 70°N and a central meridian of 45°E and the Antarctica projection will use a standard latitude of 71°S and a central meridian of 0°. Glacier products outside of Greenland and Antarctica will use region-dependent projection (e.g., UTM).

1.4.2 Tidal Displacement

Differential tidal displacement products will be produced by differencing pairs of interferograms over the ice shelves and grounding lines. This differencing approach cancels the horizontal motion (assumed constant) common to both interferograms, leaving only the double-differenced, time-varying, vertical tidal displacement, which indicates the location of the grounding line/zone, i.e. the place where ice detaches from the bed and starts becoming afloat in the ocean waters [Rignot *et al.*, 2011a; Scheuchl *et al.*, 2016]. Although this technique is generally applied to phase-only data, in the presence of very high strain rates it is possible under the right conditions to apply the technique on range offsets with a reduced level of precision in determining the grounding line position and in detecting vertical displacements [Joughin *et al.*, 2016].

1.4.3 Glacier Estimates

The mission will collect an unprecedented volume of data to measure glacier velocities in regions outside of Greenland and Antarctica. The steep terrain where many of these glaciers exist, however, present challenges (e.g., glaciers lying in radar-shadowed regions) that make it difficult to quantify what fraction of glaciers can be successfully mapped (prior measurements indicate a relatively high likelihood of success for many regions [Burgess *et al.*, 2013].) As a result, glaciers are a mission goal rather than a requirement, requiring no formal validation. (Validation efforts will still be carried out by the science team on a best effort basis.) Thus, the focus of this document is on producing ice-sheet velocity measurements. These algorithms, however, are directly applicable to mapping glaciers (actual implementations of production processors might require some modification for specific projections and other region dependent data.) Hence, throughout the remainder of the document where ice-sheet velocity mapping is referred to it is with the understanding that the text is equally applicable to glaciers (any place where this might not be the case will be so noted.)

1.5 Instrument Characteristics

All of the characteristics of the NISAR radar that were designed to optimize for interferometry are applicable to ice-sheet mapping. In particular, the 12-day repeat is well suited to ice-sheet velocity mapping. Because speckle-tracking accuracy is based on the SLC pixel dimensions, the 80-MHz mode (~2.5-m single-look ground-range resolution) will provide the best results in regions of acceptable SNR. Because NISAR's SNR degrades with bandwidth, there may be some low-backscatter regions of the ice sheet where a lower-bandwidth mode will produce better results. The algorithms described here are completely flexible with respect to bandwidth and any combination of modes can be ingested by the processor to produce results (e.g., existing implementations have produced estimates using a combination of L-, C-, and X-band data.) Note the 80-MHz mode will be employed over the ice sheets where in general a) the orbit overlap allows a half-swath mode to reduce data rate and b) there is no contention for other modes. Thus, glaciers elsewhere often will be imaged in the lower 20- or 40-MHz modes (as high resolution as possible is preferred while balancing the needs of overlapping requirements from other disciplines.)

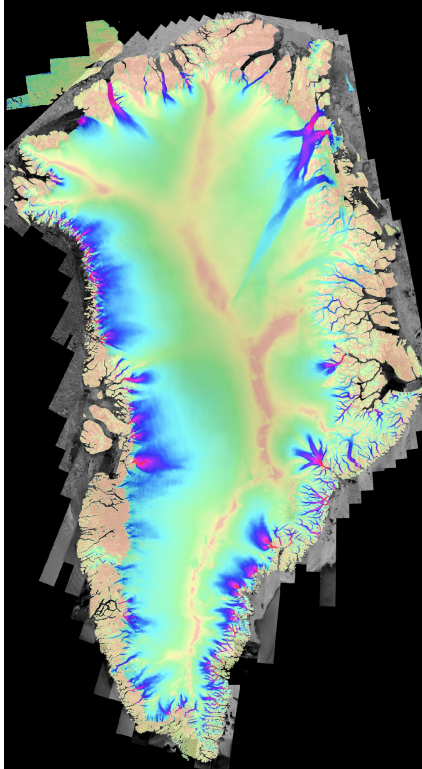


Figure 1. Example from Greenland of the type of product that will be produced using the algorithms described in this document. In the slow-moving interior velocity is derived from crossing ALOS and RADARSAT orbits. Errors do not meet NISAR requirements since there at most only a few points to average. With 30+ acquisitions a year along each track, NISAR will easily meet the stated requirements. Time series of velocity are available at <http://nsidc.org/data/measures/gimp>.

1.6 Heritage and Current Systems

Two NASA-funded production processors already exist for mapping ice-sheet velocities using SAR and they are routinely producing products under the MEaSUREs program for Greenland [Joughin *et al.*, 2010] and Antarctica [Rignot *et al.*, 2011b]. In addition, comparable systems are producing products in Europe [Nagler *et al.*, 2015]. These systems have produced ice-velocity measurements using data that extends back to the mid-1990s, using the algorithms described in this document (see Figures 1 and 2). These ongoing measurements represent an important pre-cursor data set to the NISAR mission. All of the algorithms described in this document have been implemented and have produced products by processing many thousands of SAR images from L-, C-, and X-band instruments, which have been distributed to a wide community of users (DAAC metrics indicate most of such velocity products have been downloaded by several hundred or more unique users). Thus, there is a large community ready to work with similar products developed by NISAR.

2 THEORETICAL BASIS OF ALGORITHM

The following sub-sections provide detailed descriptions of the algorithms outlined above.

2.1.1 Speckle Tracking - Caveats for Velocity Estimation

Speckle (or feature) tracked offsets are required for mapping areas of fast flow. Specifically, the L3 processor requires:

- Range and azimuth offsets computed on a relatively fine grid (~every 16 to 24 pixels in the SLC image).
- Estimates of the uncertainty in the range and azimuth offsets.
- Meta data with location and other data.

The L2 processor will compute offsets fields as a product [RD1]. For ice sheets, some additional processing may be required, which will require selecting parameters in standard algorithms [RD2] to meet ice sheet mapping requirements. First, offsets are required at much higher spatial sampling (<250 m) than is typically required for standard products. Second, computational effort scales with the search radius, which is small (a few pixels) for most areas of the Earth where there is no strong ground motion. For ice sheets, however, offsets can exceed 100 pixels or more, increasing the computational load by orders of magnitude. This load can be reduced greatly by including prior estimates of (ideally frequently updated) velocity to produce a good initial estimate of the displacement so that the search radius can be narrowed substantially. Thus, the L2 processor would benefit substantially from *a priori* velocity to help refine the search area. In addition, coherent matching can be improved if the local phase gradient is known. For most low-motion sites, this could be accomplished with a DEM. For ice sheets where there are strong phase gradients, non-standard processing where the interferogram is used can improve performance. Phase-C studies will help ascertain the best approach for the L2 production of ice-sheet offsets. For this document, we assume the L2 products have been calibrated such that baseline-dependent geometry and topographic effects have been removed (see discussion in calibration section below).

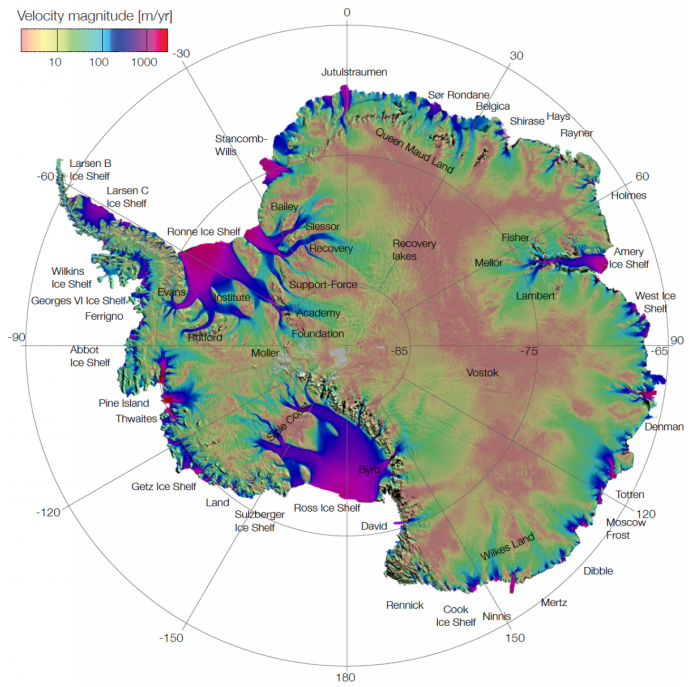


Figure 2. Example from Antarctica of the type of product that will be produced using the algorithms described in this document. With either left-only or right and left looking coverage, NISAR will map the vast interior of the Antarctic Ice Sheet. Time series of Antarctic velocity are available at <https://nsidc.org/data/measures/aiv>.

2.1.2 Interferograms – Caveats for Velocity Estimation

Ice sheet velocity and grounding line estimates derived from phase require:

- Wrapped interferogram with fine registration to account for ice sheet motion (grounding line),
- Unwrapped version of the interferogram (velocity),
- Estimate of the phase error at each point.

The standard NISAR L2 processor work flow will produce interferograms for ice velocity mapping. Because of the spatially varying displacements, fine-registration (sub-kilometer resolution) is needed in fast moving areas. Such fine registration may not be feasible or required for global processing. As a result, production of ice-sheet

velocities may require separate processing of interferograms. Any such specialized products [RD1] would use standard NISAR production code [see RD2], but with parameters optimized for fast ice flow. The L3 processor also assume the L2 products have been calibrated such that baseline-dependent geometry and topographic effects have been removed.

2.2 Definition of Quantities Used in Velocity and Grounding-Line Estimation

Velocity estimates are derived using either interferometric phase or speckle-tracked matches as described below. Here we define the notation used for the quantities that go into the velocity estimation equations.

2.2.1 Raw Speckle Tracked Offsets

At a given set of range-azimuth coordinates, (ρ_1, s_1) , in the reference SLC (first image acquired), cross correlation is used to locate same point, (ρ_2, s_2) in the second SLC, which is in non-integer values. The raw range and azimuth offsets, (δ_ρ, δ_s) , given by [ND2],

$$(1) \quad \delta_\rho = \rho_2 - \rho_1 \text{ and } \delta_s = s_2 - s_1.$$

2.2.2 Raw Interferometric Phase

Given to co-registered SLCs, I_1 and I_2 , the phase of the interferogram is given by:

$$(2) \quad \phi_w = \text{Arg}(I_1 I_2^*),$$

which is only known modulo 2π . Thus, a phase unwrapping algorithm is applied to determine the unwrapped phase, ϕ .

2.2.3 Calibrated Offsets and Phase

The interferograms and range offsets also contain information about the topography with sensitivity determined by the baseline. The imaging geometry will introduce additional displacements unrelated to surface motion. These differences can be corrected using the orbit and timing information. Here we encapsulate this information (i.e., state vectors, range delays, and any other ancillary information) into vectors, \mathbf{o}_1 and \mathbf{o}_2 , for the first and second images, respectively. With this information, then signals other than those related to surface motion can be removed to produce the surface-displacement only component of the range offset as

$$(3) \quad \delta_\rho = \delta_\rho - f_\rho(\mathbf{o}_1, \mathbf{o}_2, z),$$

Note here we assume the offsets have been scaled from pixels to units of meters. As our purpose here is to define terms rather than to provide the details of the corrections (see calibration section below), here we have bundled the geometry,

baseline, and elevation dependent corrections in a scalar function f_ρ . For now, we assume these corrections are applied in the L2 processing, but they could be applied as part of the L3 processing as described below. Similarly, we can correct the azimuth displacements in units of meters as

$$(4) \quad \delta_s = \delta_s - f_s(\mathbf{o}_1, \mathbf{o}_2).$$

The unwrapped interferometric phase, ϕ , requires similar correction such that

$$(5) \quad \Phi = \frac{4\pi}{\lambda} \delta_\rho = \phi - f_\phi(\mathbf{o}_1, \mathbf{o}_2, z),$$

which is in radians. Note this correction for phase assumes that at least one point of known speed is used as control point to determine the unknown $2 - \pi$ ambiguity associated with phase unwrapping. Such control points are routinely used in ice-sheet velocity mapping [Joughin *et al.*, 2010; Rignot *et al.*, 2011b].

2.3 Velocity Estimates at a Point

The following subsection describes how velocity is estimated at each point. Note all equations are computed assuming the look vector lies in a plane orthogonal to the satellite track (e.g., small squint). These equations have been widely used with data from a variety of sensors with no issues thus far (e.g., Figures 1&2). The imaging geometry for NISAR has low squint so that these equations should be similarly valid. As synthetic NISAR test products become available, we will examine the validity of this assumption given the more rigorous NISAR error requirements (< 1 m/yr). Should the assumption not hold, then a transformation to a squinted coordinate system would be applied to the equations below. Such a transformation, however, does not change any of the underlying principles described below nor have an impact on the viability of the algorithms, which are all well tested.

2.3.1 Ice Velocity Derived from Speckle Tracking Along a Single Orbit Track

Speckle tracking provides two components of the three-component velocity vector: the along-track horizontal component and the radar line-of-sight component, which mixes vertical and horizontal motion. Although there is a component of the vertical velocity directed toward or away from the ice-sheet surface, this motion generally is small enough (<1 m/yr) that it can be ignored or estimated independently. Instead, much of the vertical motion is due to surface-parallel flow (i.e., a particle on the surface flowing along the surface gradient) [Joughin *et al.*, 1996]. If the slope is known and surface-parallel flow can be assumed, the line-of-sight component can be resolved into horizontal and vertical components.

The line of sight displacement is given by

$$(6) \quad \delta_\rho = \Delta g \sin(\psi) - \Delta z \cos(\psi)$$

where ψ is the local incidence angle (with respect an ellipsoidal Earth), and Δz and Δg are the vertical and ground-range displacements, respectively. Solving for the horizontal displacement yields

$$(7) \quad \Delta g = \frac{\delta_p}{\sin(\psi)} + \Delta z \cot(\psi)$$

Assuming surface parallel flow, the vertical displacement is given by

$$(8) \quad \Delta z = \delta_s \frac{\partial z}{\partial s} + \Delta g \frac{\partial z}{\partial g}$$

Combining these two equations yields

$$(9) \quad \Delta g = \frac{\frac{\delta_p}{\sin(\psi)} + \delta_s \cot(\psi) \frac{\partial z}{\partial s}}{1 - \cot(\psi) \frac{\partial z}{\partial g}}$$

Using this equation and the azimuth-offset estimate the velocities in the radar-determined horizontal coordinates are given by

$$(10) \quad v_g = \frac{\Delta g}{\Delta T} \text{ and } v_s = \frac{\delta_s}{\Delta T}$$

Equation (10) gives the horizontal ice velocity in the radar-determined coordinates, but the final estimate is produced in the projection-determined xy-coordinate system (Figure 3). The rotation angle of the radar coordinates with respect to North is given by

$$(11) \quad \alpha_r = \text{atan2}\left(\frac{ds}{dlat}, \frac{dg}{dlat}\right).$$

In this equation the quantities are ds , dg are the distances in the along-track and ground-range coordinates, respectively, corresponding to an incremental poleward displacement, $dlat$. In the northern hemisphere, the rotation angle relative to north for a point (x_{PS}, y_{PS}) in polar stereographic coordinates is given by

$$(12) \quad \alpha_{PS} = \text{atan2}(y_{PS}, x_{PS}).$$

Horizontal velocities are then determined by rotating to the polar stereographic system as

$$(13) \quad \begin{bmatrix} v_x \\ v_y \end{bmatrix} = \begin{bmatrix} \cos(\alpha_{PS} - \alpha_r) & \sin(\alpha_{PS} - \alpha_r) \\ -\sin(\alpha_{PS} - \alpha_r) & \cos(\alpha_{PS} - \alpha_r) \end{bmatrix} \begin{bmatrix} v_g \\ v_s \end{bmatrix}.$$

Note the polar-stereographic coordinate system preserves angles but has a latitude-dependent scale distortion. While locations are posted in polar-stereographic coordinates, which are subject to this distortion, velocity vectors are posted in meters/year with no scale distortion.

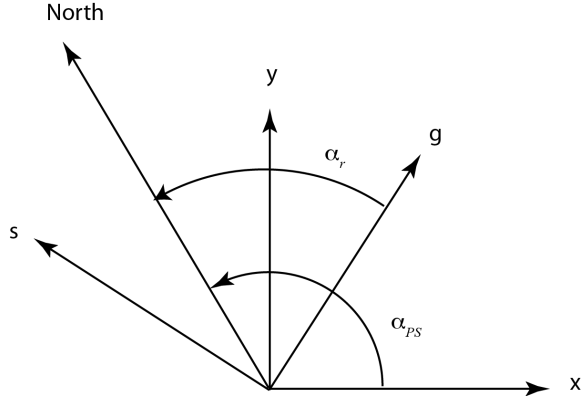


Figure 3. Radar- and projection-determined coordinate systems and their rotation angles relative to North. In the Southern Hemisphere angles are determined relative to South.

2.4 Ice Velocity Derived from Speckle Tracking and Interferometry Along Single Orbit Track

In areas where interferometric fringes are noisy or aliased so they cannot be unwrapped, speckle tracking provides a reasonable estimate. If data are available only along a single orbit track and the phase can be unwrapped, then a hybrid estimate can be derived. In this case, substituting the range displacement given by the offsets (δ_ρ) for the equivalent displacement in phase ($\lambda\Phi/4\pi$) in Equation (9) yields the surface-parallel-flow approximated ground range displacement as

$$(14) \Delta g = \frac{\frac{\lambda\Phi}{4\pi\sin(\psi)} + \delta_s \Delta_s \cot(\psi) \frac{\partial z}{\partial s}}{1 - \cot(\psi) \frac{\partial z}{\partial g}}.$$

Substituting this quantity into Equations (10) and (13) yields the horizontal velocity vector in polar-stereographic coordinates.

2.5 Ice Velocity Derived from Interferometry from Crossing Orbits with Surface-Parallel Flow

When data from crossing ascending/descending orbits are available the surface-parallel flow assumption can be used to estimate horizontal components of velocity [Joughin *et al.*, 1998; Mohr *et al.*, 1998]. Geometrically, this makes this 3-D problem a 2-D problem by assuming the velocity vector lies in the plain tangent to the

ice surface. In this case, using phase from ascending and descending passes, the horizontal components of the velocity vector are given by

$$(15) \begin{bmatrix} v_x \\ v_y \end{bmatrix} = (\mathbf{I} - \mathbf{ABC})^{-1} \begin{bmatrix} \frac{\lambda_a \Phi_a}{4\pi \Delta T_a \sin(\psi_a)} \\ \frac{\lambda_d \Phi_d}{4\pi \Delta T_d \sin(\psi_d)} \end{bmatrix}$$

where

$$(16) \mathbf{A} = \begin{bmatrix} \cos\beta & \cos(\alpha + \beta) \\ \sin\beta & \sin(\alpha + \beta) \end{bmatrix},$$

$$(17) \mathbf{B} = \left(\frac{1}{\sin\alpha} \right)^2 \begin{bmatrix} 1 & -\cos\alpha \\ -\cos\alpha & 1 \end{bmatrix} \text{ and}$$

$$(18) \mathbf{C} = \begin{bmatrix} \frac{\partial z}{\partial x} \cot(\psi_a) & \frac{\partial z}{\partial y} \cot(\psi_a) \\ \frac{\partial z}{\partial x} \cot(\psi_a) & \frac{\partial z}{\partial y} \cot(\psi_a) \end{bmatrix}.$$

In the equations quantities are as defined above with subscripts a and d to indicate whether they are from an ascending or descending pass, respectively. The angles α and β are defined in Figure 4. The incidence angles, ψ_a are ψ_d , are defined relative to an ellipsoidal Earth. A detailed derivation of these equations is given by Joughin et al. [1998].

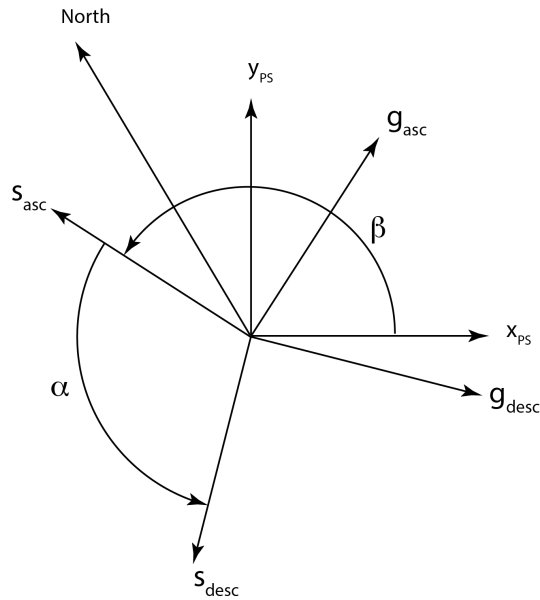


Figure 4. Definition of angles used in the computation of horizontal velocities from ascending and descending orbits. The angle between the polar stereographic x-axis and the local along-track direction is denoted by β and the angle between the ascending and descending along-track directions by α . In the Southern Hemisphere angles are determined relative to South.

2.6 Ice Velocity Derived from Speckle Tracking from Crossing Orbits with Surface-Parallel Flow

As described above, the ionosphere may introduce unacceptably large errors in some azimuth offset estimates. Range offsets are much less sensitive to ionospheric errors, so when range offsets are combined from crossing orbits, they can produce far less noisy velocity estimates. Such horizontal velocity estimates can be determined from range-offsets with the same methods as for interferometric phase. This measurement is made by replacing $\frac{\lambda_a \Phi_a}{4\pi}$ and $\frac{\lambda_d \Phi_d}{4\pi}$ in Equation (15) with $\delta_{p,a}$ and $\delta_{p,d}$, where the a and d subscripts indicate the offsets for the ascending and descending orbits, respectively.

Commented [ij1]: Note Figure 4: Fixed error where alpha and beta were swapped in the Figure.

2.7 Ice Velocity Mosaicking

The sections above describe how to measure velocity at a point given the relevant phase or offset data. Rather than point measurements, what is required for ice sheets are continental-scale mosaics stitched together from data derived from hundreds to thousands of SAR image pairs. Such algorithms are relatively mature and ice-sheet wide mosaics have already been produced from earlier sensors (e.g., Figures 1 and 2) [Joughin *et al.*, 2010; Rignot *et al.*, 2011b]. While providing a major leap forward in our understanding of ice-sheet behavior, products from existing sensors are limited in accuracy by insufficient data collection by instruments not optimized for this type of mapping. Temporal resolution of these products is also limited by a dearth of data (i.e., it took twenty years of the data from several SARs to produce a gap-free Greenland mosaic). Thus, by routinely imaging the ice sheets NISAR will greatly improve the coverage, accuracy, and spatio-temporal resolution of ice velocity estimates to help improve our understanding of how the ice sheets will contribute to sea-level change.

2.7.1 Combined Estimate

As described above, there are multiple methods for determining velocity at each point using phase or offsets from single or crossing-orbit tracks. To apply these methods, a mosaicking algorithm is needed to produce a large-scale mosaic using the best data available at each point. Here we describe an approach to mosaicking the data based on a specific implementation of a processor, which implements all of the algorithms described above to produce a mosaic [Joughin, 2002]. Variations on this approach exist but represent workflow rather than fundamental algorithmic differences [Mouginot *et al.*, 2017].

In producing such a mosaic, the algorithm proceeds by looping over the images to be mosaicked. If an estimate is being derived using data from along a single track (i.e., azimuth offsets are used), the algorithm next identifies where the corresponding region in the output grid lies, and loops over the corresponding points in the output grid. As it does this, at each point it interpolates the relevant offset or phase data from the source image, which is in radar coordinates. Where this interpolation is successful and there are valid data, the velocity components, v_x and v_y , are determined using Equations (10), (13), and (14). At each point, the algorithm uses phase data if available for the range component, and if not, then range-offset data. After looping through all points in the sub-region of output grid, the algorithm proceeds to the next image.

Where crossing orbits are used, the algorithm cycles through all of the descending (arbitrarily decided; ascending first would work just as well) images. For each of these descending images, the program then loops over all of the ascending images to determine if there is overlap. If there is overlap, then the code identifies where the region of overlap falls in the output grid. Next, the algorithm loops over these output points and computes the surface-parallel-flow approximated velocities

using Equation (15), using either phase or range-offset data. Above we have assumed that where phase data are available, they are available for both ascending and descending passes and, if not, then range-offset data are available for both passes. There can be cases, however, where range-offset data only are available from one track direction and phase data from the other. In this case, there is nothing to preclude using Equation (15) with range-offset from one track direction and phase data from the other.

As just described, for each pair or crossing pair the algorithm estimates, v_x and v_y , at each point in the output grid. For L2R-738 (coastal velocities) there may only a single estimate for most points in the output grid. By contrast, for the Requirements L2R-667 and L2R-668 (annual velocities) thirty or more independent estimates may be averaged for each point in the final output. Thus, as each point estimate is derived using image pairs, the individual estimates are weighted by w_x and w_y , summed in an output buffer. The final velocity estimate in the x-direction is derived from N individual estimates is given by

$$(19) v_x = \sum_{i=1}^N f_i w_{x,i} v_{x,i}$$

and a similar expression applies for v_y . Note f_i is an additional feathering weight as described below. If we assume the errors are unbiased (zero mean), then the weights must sum to one. In this case and assuming the individual estimates are independent, the minimum error (σ_x^2) is given by $f_i = 1$ and weights

$$(20) w_{x,i} = \frac{1}{\sigma_{x,i}^2} \left(\sum_{i=1}^N \frac{1}{\sigma_{x,i}^2} \right)^{-1}.$$

If feathering (see below) is applied ($f_i \neq 1$) then

$$(21) f_i w_{x,i} = \frac{f_i}{\sigma_{x,i}^2} \left(\sum_{i=1}^N \frac{f_i}{\sigma_{x,i}^2} \right)^{-1}.$$

In practice, the mosaicking algorithm doesn't know how many estimates are available at any given point in the output grid. As a result, it weights each estimate $v_{x,i}$ by $\frac{f_i}{\sigma_{x,i}^2}$ and sums the result in the output buffer. At the same time, a separate buffer is maintained and the weights are summed ($\sum_{i=1}^N \frac{f_i}{\sigma_{x,i}^2}$). When all data are included in the mosaic, the weighted average is completed by normalizing the final result by the summed weights.

Assuming errors are independent, then the error estimate for the weighted average is given by

$$(22) \sigma_x^2 = \sum_{i=1}^N (f_i w_{x,i})^2 \sigma_{x,i}^2 = \left(\sum_{i=1}^N \frac{f_i}{\sigma_{x,i}^2} \right)^{-2} \sum_{i=1}^N \frac{f_i^2}{\sigma_{x,i}^4} \sigma_{x,i}^2 = \left(\sum_{i=1}^N \frac{f_i}{\sigma_{x,i}^2} \right)^{-2} \sum_{i=1}^N \frac{f_i^2}{\sigma_{x,i}^2}.$$

As a result, error estimates are cumulated by summing $\frac{f_i^2}{\sigma_{x,i}^2}$ in error buffer, and the results are normalized as indicated in Equation (22).

The error estimates used in Equation (22) are derived using the equations described in the NISAR Performance Tool memo.

2.7.2 Feathering

While the weighting method described above is designed to achieve a minimum variance estimate, it may be sub-optimal with respect to other factors. For example, a discontinuity at a data-take boundary is a non-physical result and can lead to problems when attempting model inversions. As a result, additional weighting is employed to “feather” the data and redistribute local errors over a wider range. This additional weighting function is used to apply a linear taper from the edge of the data to some distance from the edge. This is accomplished by applying a distance transform that gives the distance, d , at any point in the interior to the nearest point on the image edge. The feathering function is then given by

$$(23) f(d) = \begin{cases} \frac{d}{f_l} & 0 \leq f_l \leq 1 \\ 1 & f_l \geq 1 \end{cases}.$$

This process is similar to the feathering scheme using for the SRTM mosaicking. Note the distance transform is applied to the source data, so the feather length, f_l , is in radar coordinates. This function is applied as indicated by Equation (19).

As example, if the feather length is 20, then pixels on the edge are weighted by 0, pixels within 20 pixels of the edge are weighted linearly with distance from edge over a range from 0 to 1, and interior pixels by 1. The feathering weights are used to update the initial weights in the temporary buffers, and the results are added to the weight buffers as indicated in Equation (19).

2.7.3 Final Product

At the conclusion of the mosaicking process just described, the processor outputs products with four layers: $v_x, v_y, \sigma_x, \sigma_y$. All units are in m/yr. In addition, the processor produces a meta data record, which includes information such projection, resolution, areal extent, date stamp etc.

2.8 Differential Interferogram for short-term (tidal) Motion Along a Single Orbit Track

Assuming that the dominant motion of the ice is horizontal and steady, the differencing of two interferograms spanning the same time interval and corrected for surface topography and baseline will reveal the short-term differences in the vertical motion of the ice, e.g. associated with tidal flexure of the ice if the glacier is afloat in

ocean waters or glacier surface subsidence if a subglacial lake experiences volume changes during the imaging sequence of the two interferograms. Along the ice sheet periphery, differential SAR interferograms principally reveal the vertical motion of the ice caused by changes in oceanic tide, which is the Δz term in Eq. (6) [Rignot *et al.*, 2011a]. By differencing the phase of two interferograms

$$(24) \phi_1 = \frac{4\pi}{\lambda} (\Delta g_1 \sin(\psi) - \Delta z_1 \cos(\psi)), \text{ and}$$

$$(25) \phi_2 = \frac{4\pi}{\lambda} (\Delta g_2 \sin(\psi) - \Delta z_2 \cos(\psi)),$$

Along the same track where the flow is steady such that $\Delta g_1 = \Delta g_2$, we obtain a double differential displacement as,

$$(26) \phi_1 - \phi_2 = \frac{4\pi}{\lambda} (-\Delta z_1 \cos(\psi) + \Delta z_2 \cos(\psi)) = \frac{4\pi}{\lambda} \Delta z \cos(\psi)$$

where the term, Δz , contains only differential motion associated with vertical motion. Note this term contains only the shorter-term fluctuations in the surface of the ice, with any longer-term vertical displacements (e.g., submergence/emergence velocity) common to both images canceling. Focusing on a signal associated with the short-term differences in vertical motion of the ice and assuming any horizontal motion associated with subsidence is negligible, the vertical displacement of the ice is derived as,

$$(27) \Delta z = \frac{\lambda(\phi_1 - \phi_2)}{4\pi \cos(\psi)}$$

2.9 Calibration

In the above description, the calibration terms (e.g., $f_\phi(\mathbf{o}_1, \mathbf{o}_2, z)$) are not explicitly stated to keep the focus on the L3 processing. These functions are well known and have routinely been applied to interferometric and speckle-tracked data for more than two-decades [Joughin *et al.*, 1996]. With many past sensors, the poor state vector accuracy meant that baseline parameters had to be computed using control points with known elevation and velocity. For some sensors state vectors are now accurate enough (e.g., Sentinel 1A/B) that the baseline parameters can be determined directly from the orbit reconstruction data [Nagler *et al.*, 2015]. This is the approach that will be used for NISAR, which has been validated using NISAR performance tool simulations. As noted above, Level 2 products that serve as inputs for L3 ice velocity products will need some customization of the standard production workflow to optimize the results. In developing this workflow, decisions will be made about whether it is better to apply some of these corrections as part of the L3 pre-processing rather than in L2 production. As part of this implementation effort, simulated products will be used to test and validate end-to-end (L0 through L3) production of ice velocity estimates.

3 References

- Burgess, E. W., R. R. Forster, and C. F. Larsen (2013), Flow velocities of Alaskan glaciers, *Nature Communications*, 4, doi:10.1038/ncomms3146.
- Gray, A. L., K. E. Mattar, P. W. Vachon, R. Bindschadler, K. C. Jezek, R. Forster, and J. P. Crawford (1998), InSAR results from the RADARSAT Antarctic Mapping Mission data: estimation of glacier motion using a simple registration procedure, vol. Geosci. and Rem. Sens. Proc., 1998, vol. 3, pp. 1638–1640, IEEE, Seattle.
- Joughin, I. (2002), Ice-sheet velocity mapping: A combined interferometric and speckle-tracking approach, *Ann Glaciol*, 34, 195–201.
- Joughin, I. R., R. Kwok, and M. A. Fahnestock (1998), Interferometric estimation of three-dimensional ice-flow using ascending and descending passes, *IEEE T Geosci Remote*, 36(1), 25–37.
- Joughin, I., B. E. Smith, and I. Howat (2018), Greenland Ice Mapping Project: Ice Flow Velocity Variation at submonthly to decadal time scales, *The Cryosphere*, 1–30, doi:10.5194/tc-2018-40.
- Joughin, I., B. E. Smith, I. M. Howat, T. Scambos, and T. Moon (2010), Greenland flow variability from ice-sheet-wide velocity mapping, *J Glaciol*, 56(197), 415–430.
- Joughin, I., D. E. Shean, B. E. Smith, and P. Dutrieux (2016), Grounding line variability and subglacial lake drainage on Pine Island Glacier, Antarctica, *Geophys Res Lett*, 43(17), 9093–9102, doi:10.1002/2016GL070259.
- Joughin, I., R. Kwok, and M. Fahnestock (1996), Estimation of ice-sheet motion using satellite radar interferometry: Method and error analysis with application to Humboldt Glacier, Greenland, *J Glaciol*, 42(142), 564–575.
- Michel, R., and E. Rignot (1999), Flow of Glaciar Moreno, Argentina, from repeat-pass Shuttle Imaging Radar images: Comparison of the phase correlation method with radar interferometry, *J Glaciol*, 45(149), 93–100.
- Mohr, J., N. Reeh, and S. Madsen (1998), Three-dimensional glacial flow and surface elevation measured with radar interferometry, *Nature*, 391(6664), 273–276.
- Mouginot, J., E. Rignot, B. Scheuchl, and R. Millan (2017), Comprehensive annual ice sheet velocity mapping using Landsat-8, Sentinel-1, and RADARSAT-2 data, *Remote Sensing 2017*, Vol. 9, Page 364, 9(4), 364, doi:10.3390/rs9040364.
- Nagler, T., H. Rott, M. Hetzenegger, J. Wuute, and P. Potin (2015), The Sentinel-1 Mission: New Opportunities for Ice Sheet Observations, *Remote Sensing 2017*, Vol. 9, Page 364, 7(7), 9371–9389, doi:10.3390/rs70709371.

Rignot, E., J. Mouginot, and B. Scheuchl (2011a), Antarctic grounding line mapping from differential satellite radar interferometry, *Geophys Res Lett*, 38(10), n/a–n/a, doi:10.1029/2011GL047109.

Rignot, E., J. Mouginot, and B. Scheuchl (2011b), Ice Flow of the Antarctic Ice Sheet, *Science*, 333(6048), 1427–1430, doi:10.1126/science.1208336.

Scheuchl, B., J. Mouginot, E. Rignot, M. Morlighem, and A. Khazendar (2016), Grounding line retreat of Pope, Smith, and Kohler Glaciers, West Antarctica, measured with Sentinel-1a radar interferometry data, *Geophys Res Lett*, 43(16), 8572–8579, doi:10.1002/2016GL069287.